Polymer Chemistry

ROYAL SOCIETY OF CHEMISTRY

PAPER

View Article Online
View Journal | View Issue

Cite this: *Polym. Chem.*, 2026, **17**, 347

Tunable and wavelength-gated reversible photopolymerization of quinolinone-based telechelic oligomers *via* [2π + 2π] cycloaddition

Logan Charton, [a] Richard Remy[b] and Céline Calvino *[a,b]

Received 28th October 2025,
Accepted 5th December 2025

DOI: 10.1039/d5py01021g

rsc.li/polymers

Gated photochemistry provides a powerful strategy for modulating polymer architecture under mild conditions through light-controlled reversible bond formation. Quinolinone-based photoactive units are introduced as a robust and tunable motif for reversible [2π + 2π] photocycloaddition, enabling wavelength-gated photopolymerization and depolymerization. Telechelic macromonomers bearing quinolinone end groups undergo efficient light-triggered polymerization to yield high-molecular-weight polymers ($M_p \approx 60\,000$ Da), followed by nearly complete depolymerization back to the original macromonomers under distinct irradiation wavelengths—without catalysts or additives. Systematic investigation of oxygen concentration, irradiation wavelength, and monomer concentration revealed a complex interplay governing reaction efficiency and reversibility. Oxygen enables red-shifted operation (up to 45 nm) and modulates the photostationary equilibrium, while concentration determines the balance between intermolecular chain extension and intramolecular cyclization. This wavelength- and environment-tunable photochemical response achieves reversible polymer formation, including under ambient conditions. The demonstrated tunability and reversible behavior establish quinolinone-based photoswitches as a versatile platform for recyclable and reprocessable light-responsive polymer systems.

Introduction

The development of wavelength-gated reversible covalent reactions has opened new avenues for dynamic molecular systems that can be assembled, reconfigured, or disassembled on demand using light as the sole stimulus.[1–3] This approach is particularly attractive in polymer chemistry, where precise external control over bond formation and cleavage enables the design of responsive, recyclable, or reprocessable materials. Among these light-driven transformations, [2π + 2π] cycloadditions stand out for operating without catalysts under mild conditions, offering spatial selectivity and efficient bond formation.[4,5] These reactions are typically initiated by the photoexcitation of conjugated alkenes, leading to cyclobutane formation, which can be reversed to the original alkenes upon higher-energy irradiation.[6–8] However, this approach remains limited to a narrow subset of conjugated alkenes with specific electronic structures and photochemical reactivities required for efficient [2π + 2π] cycloaddition.[9] Motifs such as coumarins,[10–12] thymines,[13–15] stilbenes,[16] maleimides,[17] cinnamic acids,[18] and styrylpyrenes[19–21] have been employed to achieve reversibility, yet even among these, few systems offer full cyclability, high fatigue resistance, and efficient bidirectional conversion (*i.e.*, cycloaddition and reversion). As a result, their implementation in fully reversible polymer systems remains rare and technically demanding, highlighting the need for new and more robust chemistries.[20,22,23]

Multiple light-controlled polymerization strategies have been explored to overcome these challenges, but most still suffer from low polymer yields, incomplete depolymerization, photofatigue, and side reactions. For instance, Chen *et al.* reported the chain extension of (polymethylenedioxy)dicoumarins in dichloromethane solution ($c = 2.5 \times 10^{-2}$ mol L^{-1}), where photoextension required up to 81 hours to reach a maximum of 78.7% conversion. Notably, benzophenone had to be employed as triplet sensitizer to enhance the photopolymerization rate. Moreover, the photodepolymerization process exhibited significant degradation as a result of side reactions that formed cleavage-resistant species accumulating over successive cycles.[24,25] Similarly, Trainor *et al.* reported a limited photoextension of telechelic polyethylene glycol (PEG)-coumarin oligomers (M_n = 4110 Da), achieving only moderate molecular weights (M_n = 8500 Da) despite extended irradiation times in the solid state. While this system displayed efficient reversibility (up to 90%), pronounced photofatigue was observed over successive cycles, further limiting

[a]*University of Freiburg, Department of Microsystems Engineering (IMTEK), Georges-Köhler-Allee 102, D-79110 Freiburg, Germany.*
E-mail: Celine.calvino@livmats.uni-freiburg.de
[b]*Cluster of Excellence livMatS, University of Freiburg (livMatS), FIT-Freiburg Center for Interactive Materials and Bioinspired Technologies, Georges-Köhler-Allee 105, D-79110 Freiburg, Germany. E-mail: Celine.calvino@livmats.uni-freiburg.de*

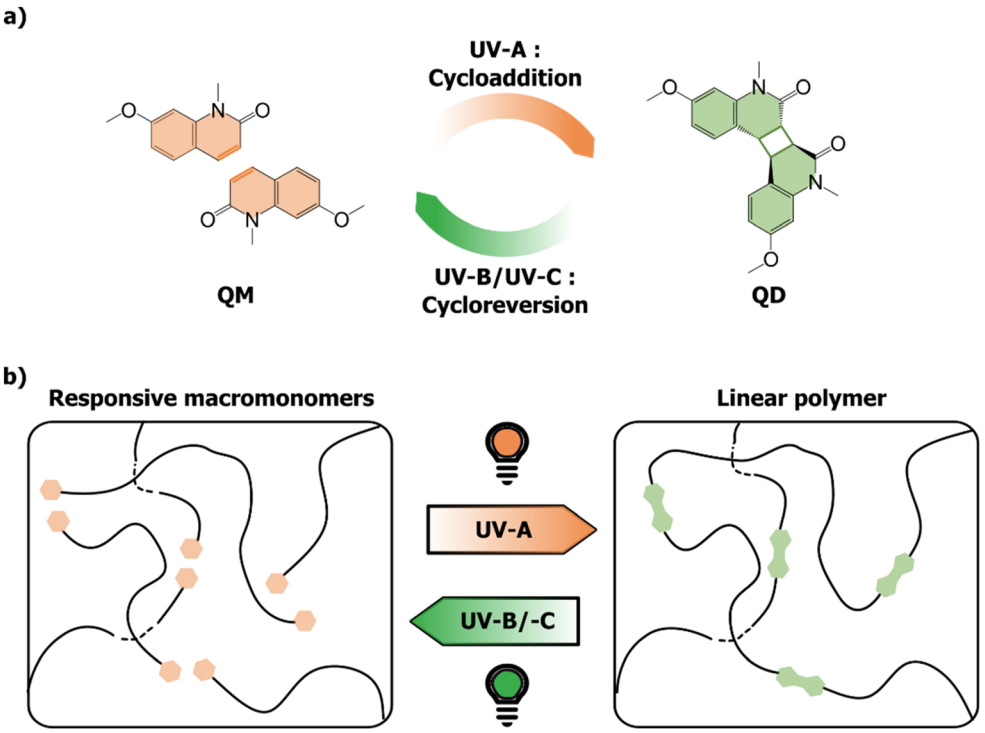

Fig. 1 (a) Schematic illustration of the reversible [2π + 2π] photocycloaddition and photocycloreversion of quinolinone photoswitches under distinct UV irradiations. (b) Schematic illustration of the reversible, covalent wavelength-gated photopolymerization and depolymerization of functional responsive macromonomers end-functionalized with quinolinone photoswitches.

material performance.[10] These issues continue to restrict the broader application of reversible photochemistry for circular polymer materials and underscore the urgent need for optimized systems featuring reduced light exposure, red-shifted operating wavelengths, and/or more robust and photoreactive photoswitches.[26,27]

While strategies such as structural modification of reactants, supramolecular templating, and the use of additives have improved the reactivity and selectivity of reversible cycloadditions, wavelength optimization *via* action plot analysis has proven to be a particularly direct and powerful approach to enhance reaction orthogonality and efficiency. Action plots correlate chemical conversion with photon flux at different wavelengths, allowing precise identification of conditions that favor either cycloaddition or cycloreversion while minimizing side reactions.[28,29] This approach facilitates more efficient, selective, and fatigue-resistant light-controlled polymerizations.

This methodology was first exemplified by Barner-Kowollik and co-workers, who employed action plot analysis on styrylpyrene derivatives to achieve highly efficient [2π + 2π] cycloaddition under blue light (435 nm) with yields exceeding 95%, as well as effective cycloreversion of up to 85% upon UV irradiation (330 nm) and notable fatigue resistance over three cycles.[20] They extended this system to monofunctional PEG macromolecules terminated with styrylpyrenes, enabling catalyst- and additive-free photoligation with conversion up to 95%.[20] Subsequently, bifunctional PEG macromonomers bearing styrylpyrene end groups were employed for wavelength-controlled reversible polymerization, yielding well-defined linear polymers with molecular weights up to M_w = 100 000 Da under optimized irradiation conditions.[30] These findings highlight the critical role of tuning both irradiation wavelength and macromonomer design to minimize macrocyclization and promote linear chain growth. Complementing these efforts, our previous work established quinolinone photoswitches as a robust scaffold for wavelength-gated [2π + 2π] reversible photochemistry (Fig. 1a).[27] Action plot analysis identified 340 nm and 265 nm as the optimal wavelengths for efficient cycloaddition and cycloreversion (under nitrogen atmosphere), respectively, enabling selective formation and reversion of a single anti-head-to-head dimer (**QD**) from *N*-methyl-quinolinone (**QM**) with near-quantitative conversion and high cyclability over eight molecular-level cycles. The system was subsequently adapted to enable photoligation of monofunctional PEG derivatives.[27]

Building on this foundation, the present study extends this system into a reversible, light-controlled polymerization platform. By incorporating these photoactive units into telechelic macromonomers, we established conditions that enabled efficient polymerization and high-efficiency depolymerization under distinct wavelengths of light—entirely without the need for catalysts or additives (Fig. 1b). Beyond achieving high conversion and maintaining structural fidelity, we further explored processing parameters to assess the

system's practical potential. Notably, conducting the process in the presence of oxygen enhanced cycloreversion efficiency and enabled red-shifted irradiation, thereby expanding the usable operating window. While depolymerization still required short wavelengths, this dual-wavelength gating strategy demonstrated a clear proof-of-concept approach toward reversible and potentially recyclable polymer architectures, highlighting the broader opportunities of quinolinone-based photoswitches for light-responsive materials.

Discussions

Condition-dependent molecular photochemical behavior

Oxygen is ubiquitous under practical conditions and can significantly affect photochemical behavior in reversible cycloaddition systems. Although its presence has been associated with substantial performance losses in the [2π + 2π] photocycloaddition of alkenes—prompting the development of various strategies to sustain reaction efficiency[31]—its role in the photoreversion pathway remains less clearly defined. Hampp and co-workers previously demonstrated that irradiation of quinolinone dimers in the presence of oxygen generates singlet oxygen, which subsequently reacts with the dimers to form endoperoxide intermediates. These intermediates then undergo oxidative cleavage, leading to irreversible by-products that disrupt cycloaddition reversibility.[26,32] Such side reactions have traditionally been viewed as detrimental, limiting the practical application of these systems under ambient conditions.

However, this singlet-oxygen-mediated pathway also offers mechanistic insight into controlled bond-cleavage processes. Because previous studies investigated only a narrow range of irradiation conditions, there remains an opportunity to systematically assess how oxygen concentration and wavelength selection influence depolymerization efficiency and side-reaction profiles. Optimizing these parameters could enable the design of oxygen-tolerant, light-responsive polymer systems with improved efficiency and durability, thereby broadening their applicability under real-world conditions.

Accordingly, the effect of oxygen on the efficiency of photocycloreversion under varying irradiation wavelengths was systematically investigated at the molecular level. Following an established protocol,[27] the extent of cycloreversion of **QD** was mapped as a function of irradiation wavelength to identify optimal conditions under ambient (oxygenated) environments (Fig. 2a). Note that **QM** and **QD** employed in these studies were synthesized according to previously reported procedures.[27,33] Solutions of **QD** in acetonitrile (ACN) (c = 3 × 10^{-5} mol L^{-1}) were irradiated in a custom-built LED photoreactor at defined wavelengths (265, 285, 310, and 325 nm), with a constant photon flux maintained across all experiments (photoreactor setup and detailed calculations are provided in the SI, section 2.1.8 and 2.2.4). Reaction conversions were monitored and quantified using UV-vis spectroscopy (Fig. S1, see SI, section 2.2.2 and 2.2.3). Consistent with our previous study, high reactivity was observed under 265 nm irradiation. However, a distinct and reproducible increase in photocycloreversion efficiency was observed when reactions were conducted in the

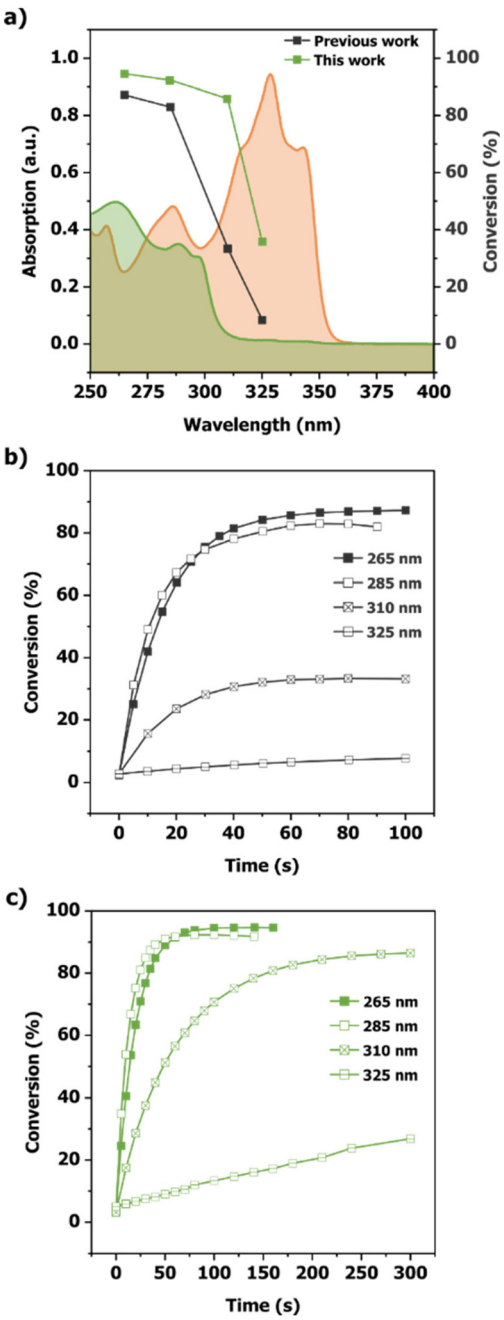

Fig. 2 (a) Action plots obtained for the cycloreversion of **QD** with irradiations of 6.09 × 10^{19} photons at different wavelengths (265 nm, 285 nm, 310 nm, 325 nm), under oxygen-free conditions (black square) and under oxygenated conditions (green square), as well as the UV-vis spectra of **QM** (orange) and **QD** (green). (b) Comparison of the photocycloreversion conversions of **QD** over time under irradiation at 265, 285, 310, and 325 nm under oxygen-free conditions. (c) Comparison of the photocycloreversion conversions of **QD** over time under irradiation at 265, 285, 310, and 325 nm under oxygenated conditions. Photoreactions were carried out in ACN solutions at c = 3 × 10^{-5} mol L^{-1} and irradiated with an LED photoreactor operating at power levels ranging from 22 to 80 mW.

presence of oxygen (Fig. 2a), particularly at longer wavelengths (*i.e.*, 285 and 310 nm) where analogous kinetics conducted under inert conditions yielded limited reactivity. Specifically, kinetic analysis under oxygen-free conditions revealed moderate reaction rates of 0.04627 and 0.05435 s^{-1} with conversions reaching up to 95% at 265 and 285 nm, followed by a marked decline in both rate and overall conversion at longer red-shifted wavelengths (Fig. 2b and Fig. S2a–c for rates calculations). This decline in conversion is attributed to the establishment of a photostationary-state equilibrium, in which the photocycloreversion of the cyclobutanes competes with the photocycloaddition of the generated alkenes.[5,34,35] The equilibrium effect becomes more pronounced when irradiation occurs in regions where the UV absorption bands of the alkene and cyclobutane moieties overlap, thereby limiting the net forward reaction. Importantly, UV-Vis absorption spectra of oxygen-rich and oxygen-free samples exhibited identical pattern (Fig. S3a), indicating that the enhanced reactivity in oxygen does not arise from changes in optical absorption. In contrast, irradiation in the presence of oxygen resulted in modestly higher reaction rates—1.04 to 1.46 times greater across all tested wavelengths—while maintaining high conversion levels (up to 95%) (Fig. 2b and c). Most strikingly, efficient photocycloreversion was achieved at 310 nm—a wavelength previously ineffective under inert conditions—now yielding over 90% conversion with an appreciable reaction rate of 0.01455 s^{-1}. For all kinetic experiments, high-performance liquid chromatography (HPLC) analysis of the irradiated solutions, collected at the conversion plateau after 2–50 minutes of irradiation, consistently showed exclusive formation of **QM** with no detectable side-products, in agreement with previous reports (Fig. S3b and c).[27]

These observations point toward a distinct mechanistic pathway in the presence of oxygen. The enhanced reactivity at red-shifted wavelengths, which is absent under nitrogen, suggests a photosensitized mechanism likely involving singlet oxygen. This interpretation supports Hampp's earlier hypothesis that *in situ*-generated singlet oxygen facilitates cleavage of the cyclobutane ring.[26] Such oxygen-mediated pathways—whether through singlet-oxygen generation or modified excited-state relaxation dynamics, including increased intersystem crossing—open additional photochemical channels that accelerate bond cleavage and improve overall reactivity.[26] In contrast, oxygen is known to interfere with the cycloaddition process by quenching the triplet excited state of the alkene, thereby suppressing dimer formation.[36] This inhibitory effect is evident from kinetic experiments, where even trace amounts of oxygen cause up to a sixteen-fold decrease in cycloaddition rates compared to inert conditions (Fig. S4a–c), consistent with previous observations in [2π + 2π] photocycloadditions.[30] This suppression effectively shifts the photostationary equilibrium toward the monomeric form under oxygen conditions.

Importantly, the ability to efficiently trigger depolymerization at lower-energy wavelengths presents a substantial advantage by reducing reliance on high-energy UV irradiation, which is often associated with photodamage and limited material compatibility.[37,38] This oxygen-assisted photocycloreversion therefore represents a promising route toward more practical and environmentally compatible light-responsive polymer systems, capable of operating under ambient conditions. Moreover, these findings highlight the importance of conducting action plot analysis, as it captures the intricate interplay between oxygen, wavelength, and photoreactivity that might otherwise be overlooked. Such detailed investigations are essential for accurately understanding and optimizing light-driven processes.

Interestingly, repeated experiments conducted under ambient oxygen conditions revealed notable variability in reaction efficiency (Fig. S5), suggesting that fluctuations in dissolved oxygen concentration—arising from subtle differences in sample handling or preparation—may influence the reversion process. This observation supports the notion that oxygen does not merely act as a passive background component but rather plays an active role in the photoreaction mechanism.

To further assess the effect of oxygen concentration, a series of kinetic experiments was conducted under systematically varied relative oxygen levels while maintaining constant photon flux and sample concentration. Samples were prepared under nitrogen-purged conditions ("0%"), oxygen-rich conditions generated by saturating the solution with ambient air, and intermediate relative oxygen levels ("rel. 25%", "rel. 50%", and "rel. 75%") obtained by mixing the oxygen-rich and nitrogen-purged solutions (see SI, section 2.2.5). These values represent relative mixtures rather than absolute dissolved-oxygen concentrations. All samples were irradiated at 310 nm (80 mW) for intervals of time ranging from 10 seconds to 720 minutes. The resulting conversion profiles (Fig. 3a) exhibited a clear dependence on oxygen content. Although reaction rates remained largely unchanged, the final conversion increased progressively with higher relative oxygen levels. Under oxygen-rich (ambient-air-saturated) conditions, the reaction reached a final conversion of 91%, compared to only 30% under oxygen-free conditions ("0%"), confirming the role of oxygen in facilitating the reversion. At higher relative oxygen levels, a subsequent decline in conversion was observed after reaching a plateau, indicating side-product formation under prolonged irradiation.

To monitor the progression of the reversion reaction and identify potential side products, HPLC analysis was performed at defined time points during irradiation under oxygen-rich (ambient-air–saturated) conditions (Fig. 3a and b). The chromatograms revealed a clean transition from **QD** to **QM**, reaching maximum conversion after 5 minutes (Fig. 3b). Beyond this point, new peaks emerged, consistent with side-product formation and the decline in conversion observed in the kinetic profiles. These results indicate that the reversion proceeds with high selectivity up to a certain extent, and that reaction time can serve as a control parameter to favor the recovery of the original monomer.

This concept was further validated through light-induced cycling of the dimer, with cycloreversion triggered at 310 nm under oxygen-rich conditions and cycloaddition induced at 340 nm under oxygen-free conditions. The cycloaddition step

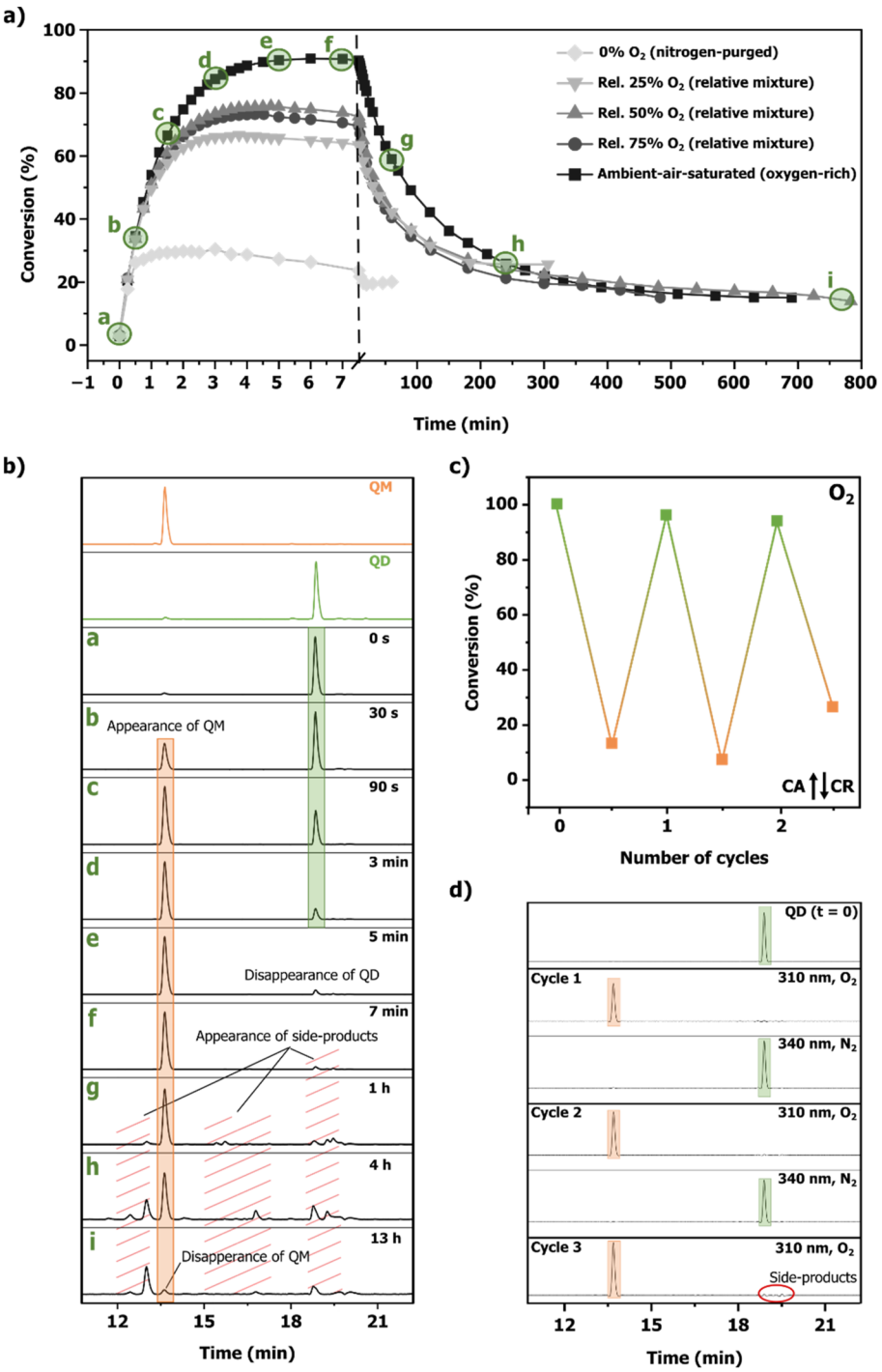

Fig. 3 (a) Conversion profiles over time for the cycloreversion of **QD** to **QM** under nitrogen-purged ("0%"), oxygen-rich (ambient-air–saturated), and intermediate relative oxygen levels (rel. 25–75%). (b) Comparison of HPLC chromatograms for pure **QM** (orange), pure **QD** (green), and irradiated samples collected at different time points during the cycloreversion of **QD** at 310 nm under oxygen-rich conditions (ambient-air–saturated, black). The chromatographic data correspond to the kinetic profiles (a–i) shown in panel (a). (c) Subsequent irradiation cycles of **QD** conducted at 310 nm under oxygen-rich conditions for the cycloreversion (CR, from green to orange) and at 340 nm under oxygen-free conditions for the cycloaddition (CA, from orange to green). (d) Comparison of the HPLC chromatograms of **QD** at t = 0 (green), and from each step of the **QD**/**QM** cyclization experiments described in panel (c). The photoreactions were carried out in ACN solutions at $c = 3 \times 10^{-5}$ mol L^{-1} using an LED photoreactor at power levels ranging from 33 to 80 mW.

was carefully performed under an inert atmosphere to prevent oxygen-induced side reactions and associated performance losses. Hampp and co-workers previously demonstrated that in the presence of oxygen, photooxidation of the anti-head-to-head *N*-methyl-quinolinone dimer generates bis-*N*-methyl-quinolinone (bis-NMQ), which severely limits the reversibility of the motif (Fig. S6).[32] Consistent with these findings, conducting both photoprocesses entirely under oxygen in our system resulted in a rapid loss of cyclability due to oxidative degradation and side-product formation, as confirmed by UV-vis and HPLC analyses (Fig. S7a and b). Accordingly, both reactions were carried out in a one-pot setup following established protocols ($c = 3 \times 10^{-5}$ mol L^{-1}). Cycloaddition and cycloreversion were performed under nitrogen and oxygen, respectively, using the previously determined irradiation parameters, and conversions were extracted from absorption changes (Fig. S8). Under these optimized conditions, the system displayed reversible switching between **QD** and **QM** across at least two cycles, with spectral and chromatographic data indicating good retention of signal patterns (Fig. 3c and d). Minor fatigue observed after the third cycle is likely associated with experimental handling during the switching of gaseous environments rather than intrinsic degradation of the system. Cumulative solvent losses during these atmosphere changes lead to a gradual increase in concentration, which in turn slightly affects reaction rates and the kinetics of by-product formation identified in earlier experiments. Furthermore, as a control experiment, following an initial cycle comprising cycloreversion in the presence of oxygen (310 nm) and cycloaddition under nitrogen (340 nm), cyclization performed entirely under oxygen-free conditions (at 265 and 340 nm) demonstrated efficient system cyclability (Fig. S9a). The UV-vis spectra exhibited a pattern closely resembling the cyclization behavior of **QD** and **QM** under strictly inert conditions (at 265 nm and 340 nm) (Fig. S9b), thereby confirming that the previously observed loss of cyclability originates from technical factors rather than intrinsic degradation of the system. This finding further supports the potential for controlled monomer recovery *via* photoreversion and highlights the suitability of these photoresponsive motifs for integration into light-responsive materials, provided that irradiation conditions are optimized to minimize degradation.

Reversible photopolymerization under oxygen-free conditions

Building on the preceding molecular studies, the system was extended to the macromolecular level to enable reversible and orthogonal photopolymerization of functional building blocks (Fig. 4a). Following established protocols,[27,39,40] commercially available α,ω-bis-amino PEG (nominal M_n = 6000 Da, measured $M_{n,\,exp}$ = 5600 Da) was end-functionalized with quinolinone units to afford the bis-functional macromonomer **QM-PEG-QM** (see SI, section 2.3). PEG was selected as the polymer backbone owing to its well-established role as a model matrix in photoligation chemistry and its synthetic versatility.[20,41] Successful end-group functionalization was confirmed by ^{1}H-NMR spectroscopy, which showed a downfield shift of the methylene protons α to the amine groups, from 2.86 to 3.35 ppm, consistent with urea formation, as well as the emergence of characteristic quinolinone aromatic signals between 8.50 to 6.00 ppm. Additionally, gel permeation chromatography (GPC) revealed an increase in molecular weight to M_n = 7097 Da (see Supporting Molecular Characterization). To further validate the introduction of the quinolinone motif, GPC with UV and differential refractive index (dRI) detection showed overlapping UV and dRI traces at a peak molecular weight of M_p = 12 365 Da (Fig. S10). The chromatogram exhibited a bimodal profile, attributed to partial dimerization of the telechelic monomer due to ambient light exposure or UV irradiation during analysis—an occurrence previously reported.[10,27] Additional confirmation of quinolinone incorporation came from the UV-vis absorption spectrum of the polymer, which showed a clear maximum at λ_{max} = 328 nm, characteristic of the quinolinone chromophore (Fig. S11).

As an initial demonstration, and building on previous molecular studies showing effective cyclability, photopolymerization was performed under fully oxygen-free conditions in ACN (c = 50 mg mL^{-1}), using irradiation at 340 nm for 25 minutes. Reaction aliquots were collected at different intervals (2–10 minutes) and analyzed by UV-vis spectroscopy and GPC. The absorption spectra showed a gradual decrease in the quinolinone band accompanied by the emergence of the dimer signal, reaching a plateau after approximately 20 minutes (Fig. S12). This behavior indicates the attainment of maximum photoconversion under the applied conditions, with the overall conversion of ~97%. In parallel, GPC analysis revealed progressive molecular weight growth, reaching $M_p \approx 60\,000$ Da with a broad dispersity ($Đ > 1.92$), consistent with a step-growth polymerization mechanism (Fig. 4b).[30,42] The elution profile exhibited a tail-heavy distribution, reflected by the substantial differences between number-average (M_n = 19 700 Da), weight-average (M_w = 37 900 Da) and z-average (M_z = 53 500 Da) molecular weights. ^{1}H-NMR spectroscopy further confirmed successful photoextension, showing complete disappearance of the quinolinone vinylic protons at 7.61–7.59 and 6.57–6.54 ppm and the appearance of characteristic cyclobutane proton resonances at 3.69 ppm (Fig. S13a and b).

The *N*-methyl protons also shifted from 3.67 to 3.42 ppm, consistent with previous observations of quinolinone dimerization.[27] Collectively, these results demonstrate near-quantitative conversion of the macromolecular precursors and formation of well-defined, extended linear polymers.

Further experiments at lower macromonomer concentrations (c = 0.33 mg mL^{-1}) revealed a marked shift in the polymerization outcome, favoring the formation of smaller cyclic species rather than extended linear chains (Fig. S14). This behavior arises from the inherent concentration dependence of step-growth polymerization: at low concentrations, intramolecular cyclization becomes more probable than intermolecular chain extension, thereby limiting achievable molecular weights.[30,43] Interestingly, despite the reduced chain growth, the overall reaction rate increased under these dilute conditions, likely due to a higher photon-to-molecule ratio enhancing excitation efficiency. However, this acceleration did

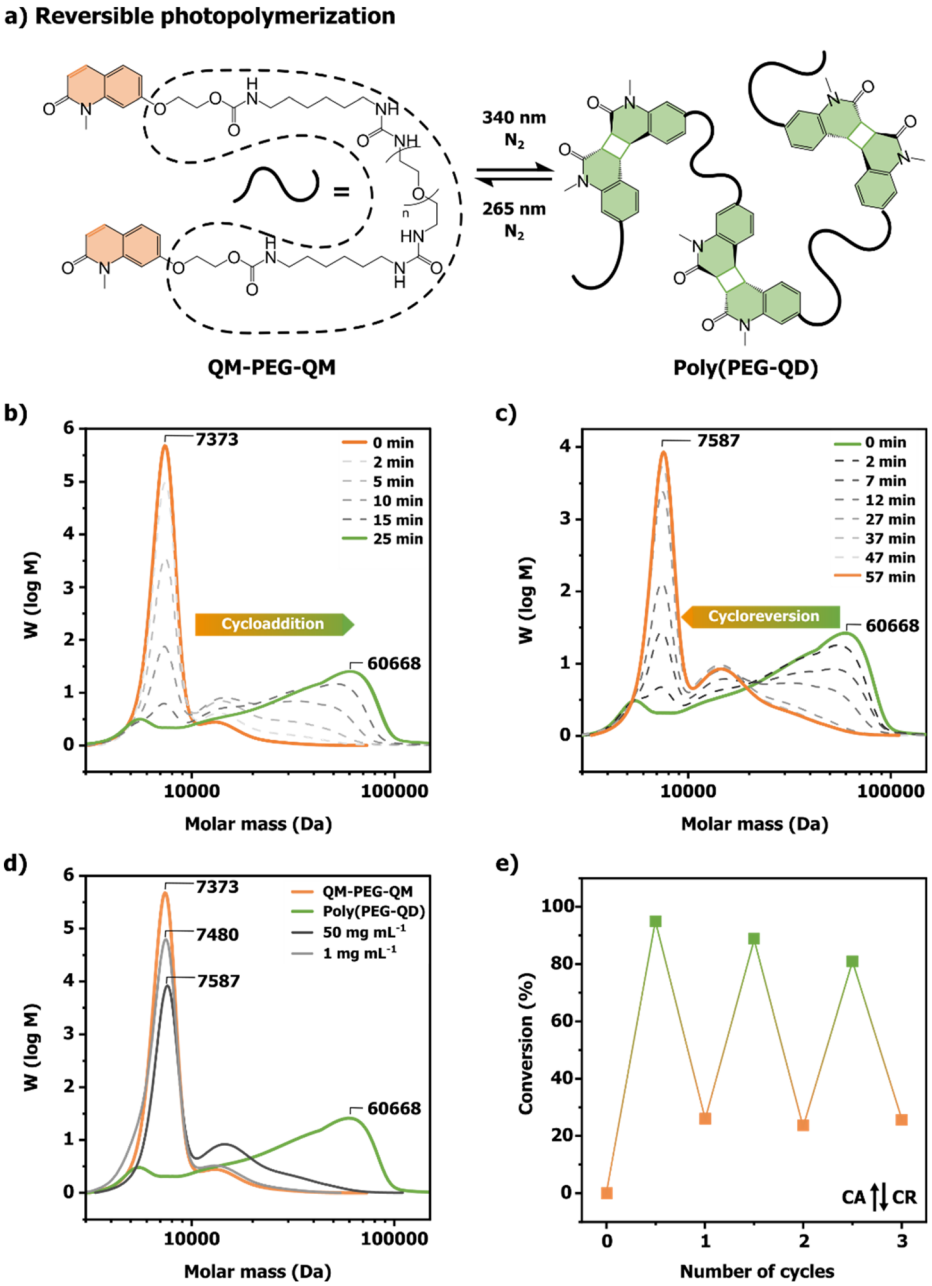

Fig. 4 (a) Schematic representation of the reversible formation of **poly(PEG-QD)** through an orthogonally triggered [2π + 2π] photocycloaddition (340 nm) and photocycloreversion (265 nm) under oxygen-free conditions. (b) GPC chromatograms from the [2π + 2π] photocycloaddition of **QM-PEG-QM** (c = 50 mg mL^{-1}), conducted at 340 nm under oxygen-free conditions, at different irradiation times. (c) GPC chromatograms from the [2π + 2π] photocycloreversion of **poly(PEG-QD)** (c = 50 mg mL^{-1}), conducted at 265 nm under oxygen-free conditions, at different irradiation times. (d) GPC chromatograms from the [2π + 2π] photocycloreversion of **poly(PEG-QD)**, conducted at 265 nm under oxygen-free conditions, at c = 50 mg mL^{-1} (grey) and at c = 1 mg mL^{-1} (black). (e) Subsequent irradiation cycles of **QM-PEG-QM** (c = 50 mg mL^{-1}) conducted at 340 nm (25 min) for cycloaddition (CA, from orange to green) and at 265 nm (45 min) for cycloreversion (CR, from green to orange), under oxygen-free conditions. The photoreactions were carried out in ACN solutions using an LED photoreactor at power levels ranging from 22 to 33 mW.

not yield longer polymer chains but instead promoted cyclic oligomer formation, as evidenced by a distinct peak at M_p = 5400 Da in the GPC trace. This observation aligns with previous reports of concentration-dependent cyclization in telechelic systems (Fig. S15).[43–45] Finally, it is worth noting that the maximum usable concentration was constrained by the solubility limit of **QM-PEG-QM** in ACN (50 mg mL^{-1}), restricting further optimization toward higher molecular weights.

Subsequently, depolymerization of the extended polymer was performed at 265 nm under oxygen-free conditions. At high concentration (c = 50 mg mL^{-1}), UV-vis spectroscopy

revealed substantial bond cleavage, with ~78% conversion achieved after 47 minutes of irradiation, followed by a reaction plateau (Fig. S16). In parallel, GPC analysis confirmed the breakdown of the polymer into its original macromonomers, along with a measurable fraction of dimers (Fig. 4c). Complementary ^{1}H-NMR analysis supported the regeneration of the macromonomer, revealing the expected quinolinone signals alongside additional resonances consistent with dimers (~22%, Fig. S13c). A higher degree and rate of depolymerization were achieved by lowering the concentration to c = 1 mg mL^{-1}, resulting in additional cleavage of dimers into macromonomers after 4 min of irradiation, as evidenced by the near-complete recovery of the original chromatographic profile at M_p = 7480 Da ($Đ$ = 1.15), along with the reappearance of the characteristic quinolinone absorption bands in the UV-vis spectra (Fig. 4d and Fig. S17). At this low concentration, GPC also revealed the emergence of a distinct lower-molecular-weight shoulder (Fig. 4d), attributed to the formation of macrocyclic species. Similar features have been reported previously,[30,43] and are attributed to dilution-induced intramolecular cyclization during photochemical depolymerization under photostationary equilibrium. In such cyclic architectures, the proximity of reactive motifs stabilizes this equilibrium and restricts conformational freedom, thereby hindering complete bond scission.

Finally, combining photopolymerization and depolymerization under optimized conditions (340 nm and 265 nm, respectively, at high concentration, c = 50 mg mL^{-1}) produced reversible behavior, as evidenced by three consecutive switching cycles with good retention of spectral and chromatographic fidelity (Fig. 4e and Fig. S18). A gradual decrease in performance was observed over successive cycles, which manifested primarily as reduced cycloaddition efficiency. This trend is consistent with partial photodegradation during the reversion step, leading to a progressively smaller fraction of fully regenerable reactive components. As previously noted, performing the photoreversion at lower concentration shortens irradiation times and significantly mitigates degradation, although it cannot eliminate it entirely.

Taken together, these results demonstrate that quinolinone-based macromonomers enable efficient, reversible, and nearly orthogonal photopolymerization, marking their first successful application in recyclable polymer systems. The demonstrated efficiency, fidelity, and responsiveness establish quinolinone-based photoswitches as a strong and versatile platform within the broader landscape of photoresponsive polymer architectures.[30,43,46]

Depolymerization under oxygenated conditions

Building on the efficient depolymerization achieved under oxygen-free conditions, the robustness of the process was examined under less stringent and more practically relevant conditions, specifically in an aerobic environment. Solutions were prepared as previously described (ambient-air-saturated, see SI, section 2.2.12), and the photoextended polymer **poly (PEG-QD)** was subjected to red-shifted irradiation (310 nm) under ambient atmospheric conditions. At high concentration (c = 50 mg mL^{-1}), the reaction exhibited limited conversion, reaching only 33% after 25 minutes of irradiation, as determined by UV-vis spectroscopy (Fig. 5a). Prolonged exposure led to visible sample degradation, consistent with earlier molecular studies that identified side products after 7 minutes of irradiation in the presence of oxygen (Fig. 3b). However, decreasing the concentration to c = 1 mg mL^{-1} or below increased the reaction rate, yielding a conversion plateau of 60% within 5 minutes of irradiation. Corresponding GPC analysis revealed extensive depolymerization accompanied by the presence of dimeric and macrocyclic monomer fractions,

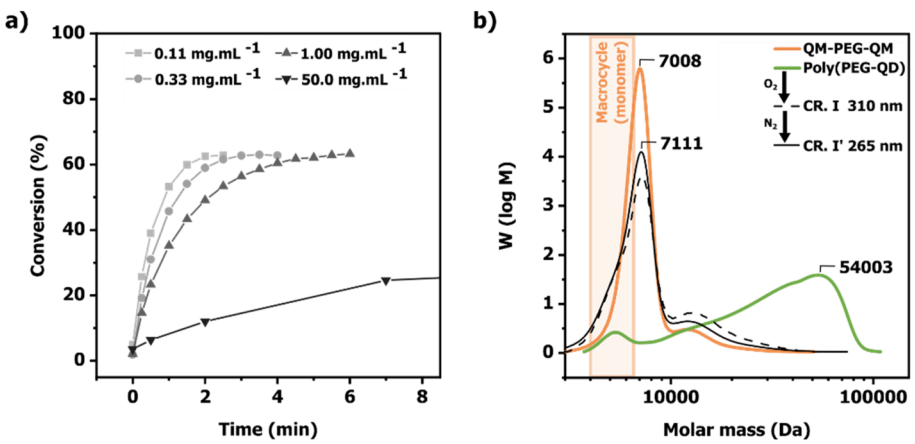

Fig. 5 (a) Comparison of the conversions over time of the cycloreversion of **poly(PEG-QD)** into **QM-PEG-QM** through irradiation at 310 nm under oxygenated conditions for different concentrations (from 0.11 to 50 mg mL^{-1}) of **poly(PEG-QD)**. (b) Comparison of the GPC chromatograms of **QM-PEG-QM** (orange line), **poly(PEG-QD)** (green line), the cycloreversion (CR.I) of **poly(PEG-QD)** through irradiation at 310 nm under oxygenated conditions at c = 0.33 mg mL^{-1} (black dashed line), and the follow-up irradiation (CR.II) at 265 nm under oxygen-free conditions, at c = 0.33 mg mL^{-1} (black solid line). The photoreactions were carried out in ACN solutions using an LED photoreactor at power levels ranging from 60 to 80 mW.

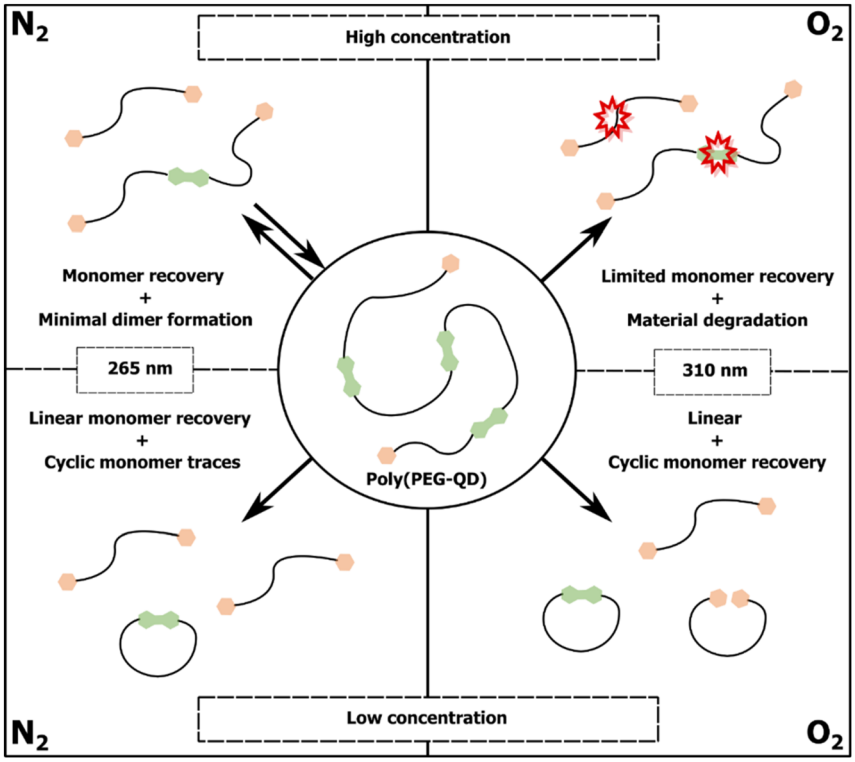

Fig. 6 General overview of the building block recovery possibilities during the depolymerization of **poly(PEG-QD)** from the interplay between the wavelengths (from left to right), the atmosphere (N_2/O_2), and the concentration (from top to bottom).

together accounting for approximately 40% based on UV quantification (Fig. 5a and b). This improvement is attributed to the wavelength shift, which lowers the photon flux and thereby modifies reaction dynamics. Note that a similar concentration dependence was also observed in the small-molecule system, where dilution increased the efficiency of photocycloreversion (Fig. S19a). Overall, the results highlight a complex interplay between concentration, irradiation time, wavelength, and reaction rate, all of which critically govern the photochemical equilibrium between linear polymers and macrocyclic species.

With this understanding, irradiation at 265 nm under nitrogen reduced the photostationary equilibrium effect between linear polymers, dimers and macrocycles, allowing further recovery of macromonomers. This effect was confirmed by UV-vis spectroscopy, which showed a 10% increase in depolymerization conversion before the system reached a new equilibrium. Moreover, drawing on molecular-level observations that oxygen inhibits the cycloaddition reaction, irradiation at 265 nm under oxygen shifted this equilibrium even further, achieving up to a 20% increase in conversion (Fig. S19b). These findings indicate that, although macrocycles form during depolymerization, they remain cleavable under optimized conditions, and emphasize the intricate interdependence of concentration, irradiation time, wavelength, and environmental factors in controlling polymer reversibility.

Conclusion

The photocycloreversion efficiency of the quinolinone dimer is governed by the combined effects of three key parameters: oxygen concentration, irradiation wavelength, and monomer concentration. Oxygen modulates the kinetics of the cycloaddition and cycloreversion processes, thereby mitigating the effects of the photostationary state and enhancing conversion at longer wavelengths (≥310 nm). At the same time, oxygen can trigger competing photochemical pathways that influence both efficiency and selectivity. However, excessive irradiation under oxygenated conditions promotes side-product formation and reduces selectivity. Optimal depolymerization can nonetheless be achieved under ambient oxygen levels through appropriate control of the irradiation time. Wavelength plays a decisive role in determining the reaction pathway: short wavelengths (<300 nm) efficiently induce cycloreversion even under inert conditions, whereas longer wavelengths require oxygen to reach comparable performance. Macromonomer concentration dictates the balance between polymer growth and macrocyclization, with higher concentrations favoring polymerization and lower concentrations promoting intramolecular ring formation.

Overall, the study demonstrates that the motif's behavior arises from a complex, synergistic interplay of structural features, environmental factors, and external stimuli. These parameters act collectively to define the system's photochemi-

cal response. This interplay (summarized in Fig. 6) provides a practical framework for selecting conditions that maximize conversion, minimize by-products, and tailor polymer architecture. The quinolinone motif exhibits robust and tunable photochemical behavior, offering a versatile platform for reversible photopolymers. While the requirement for short wavelengths imposes limitations for long-term cycling, the demonstrated switching performance across diverse environments highlights the mechanistic potential of this class of photoswitches. By strategically modulating key parameters, the system can be adapted to specific functional demands and provides a foundation for future development of light-responsive and potentially recyclable polymer materials.

Conflicts of interest

The authors declare no competing financial interest.

Data availability

All data supporting the findings of this study are available in the supplementary information (SI) accompanying this article. Supplementary information is available. See DOI: https://doi.org/10.1039/d5py01021g.

Acknowledgements

The authors gratefully acknowledge the help of Natalia Schatz for conducting the GPC measurements, Sascha Ferlaino for conducting the NMR experiments as well as Dr Claas-Hendrik Stamp and Jana Stumpp for their valuable scientific and technical support. The authors also gratefully acknowledge financial support through the Deutsche Forschungsgemeinschaft (DFG, German Research Foundation) under Germany's Excellence Strategy – EXC-2193/1-390951807 and through the Baden-Württemberg Stiftung, project BWST-ISF2020-12.

References

1 V. X. Truong and C. Barner-Kowollik, *Trends Chem.*, 2022, **4**, 291–304.
2 Y. Huang, X. Wang, J. Li, Y. Lin, H. Chen, X. Liu and X. Huang, *ChemSystemsChem*, 2021, **3**, e2100006.
3 O. Bertrand and J.-F. Gohy, *Polym. Chem.*, 2017, **8**, 52–73.
4 C. Cardenas-Daw, A. Kroeger, W. Schaertl, P. Froimowicz and K. Landfester, *Macromol. Chem. Phys.*, 2012, **213**, 144–156.
5 H. Frisch, D. E. Marschner, A. S. Goldmann and C. Barner-Kowollik, *Angew. Chem., Int. Ed.*, 2018, **57**, 2036–2045.
6 T. Bach, *Synthesis*, 1998, **1998**, 683–703.
7 S. Poplata, A. Tröster, Y.-Q. Zou and T. Bach, *Chem. Rev.*, 2016, **116**, 9748–9815.
8 M. Jiang, N. Paul, N. Bieniek, T. Buckup, N. Hampp and M. Motzkus, *Phys. Chem. Chem. Phys.*, 2017, **19**, 4597–4606.
9 P. Klàn and W. Jakob, in *Photochemistry of Organic Compounds*, 2009, pp. 227–453.
10 S. R. Trenor, T. E. Long and B. J. Love, *Macromol. Chem. Phys.*, 2004, **205**, 715–723.
11 M. Nagata and Y. Yamamoto, *J. Polym. Sci., Part A:Polym. Chem.*, 2009, **47**, 2422–2433.
12 G. Kaur, P. Johnston and K. Saito, *Polym. Chem.*, 2014, **5**, 2171–2186.
13 M. J. Moghaddam, S. Hozumi, Y. Inaki and K. Takemoto, *J. Polym. Sci., Part A:Polym. Chem.*, 1988, **26**, 3297–3308.
14 N. Tohnai, T. Sugiki, E. Mochizuki, T. Wada and Y. Inaki, *J. Photopolym. Sci. Technol.*, 1994, **7**, 91–92.
15 E. Mochizuki, N. Tohnai, Y. Wang, T. Saito, Y. Inaki, M. Miyata, N. Yasui and Y. Kai, *Polym. J.*, 2000, **32**, 492–500.
16 A. P. Somlai, R. A. Cozad, K. A. Page, H. R. Williams, D. Creed and C. E. Hoyle, *Photochem. Photobiol. Sci.*, 2008, **7**, 578–587.
17 M. Aljuaid, Y. Chang, D. M. Haddleton, P. Wilson and H. A. Houck, *J. Am. Chem. Soc.*, 2024, **146**, 19177–19182.
18 D. Shi, M. Matsusaki, T. Kaneko and M. Akashi, *Macromolecules*, 2008, **41**, 8167–8172.
19 T. Doi, H. Kawai, K. Murayama, H. Kashida and H. Asanuma, *Chem. – Eur. J.*, 2016, **22**, 10533–10538.
20 D. E. Marschner, H. Frisch, J. T. Offenloch, B. T. Tuten, C. R. Becer, A. Walther, A. S. Goldmann, P. Tzvetkova and C. Barner-Kowollik, *Macromolecules*, 2018, **51**, 3802–3807.
21 V. X. Truong, F. Li, F. Ercole and J. S. Forsythe, *ACS Macro Lett.*, 2018, **7**, 464–469.
22 D. Kehrloesser, R.-P. Baumann, H.-C. Kim and N. Hampp, *Langmuir*, 2011, **27**, 4149–4155.
23 J. Jiang, B. Qi, M. Lepage and Y. Zhao, *Macromolecules*, 2007, **40**, 790–792.
24 Y. Chen and C.-S. Jean, *J. Appl. Polym. Sci.*, 1997, **64**, 1749–1758.
25 Y. Chen and C.-S. Jean, *J. Appl. Polym. Sci.*, 1997, **64**, 1759–1768.
26 N. Bieniek, S. Inacker and N. Hampp, *Phys. Chem. Chem. Phys.*, 2021, **23**, 17703–17712.
27 M. Streicher, C.-H. Stamp, M. D. Kluth, A. Ripp and C. Calvino, *Macromol. Rapid Commun.*, 2024, **45**, 2400474.
28 I. M. Irshadeen, S. L. Walden, M. Wegener, V. X. Truong, H. Frisch, J. P. Blinco and C. Barner-Kowollik, *J. Am. Chem. Soc.*, 2021, **143**, 21113–21126.
29 I. M. Irshadeen, K. De Bruycker, A. S. Micallef, S. L. Walden, H. Frisch and C. Barner-Kowollik, *Polym. Chem.*, 2021, **12**, 4903–4909.
30 H. Frisch, K. Mundsinger, B. L. J. Poad, S. J. Blanksby and C. Barner-Kowollik, *Chem. Sci.*, 2020, **11**, 2834–2842.
31 J. C. G. Kürschner, L. Brüss and L. Næsborg, *Chem. – Eur. J.*, 2023, **29**, e202300627.
32 N. Bieniek, C. P. Haas, U. Tallarek and N. Hampp, *Photochem. Photobiol. Sci.*, 2021, **20**, 773–780.

33 N. Paul, M. Jiang, N. Bieniek, J. L. P. Lustres, Y. Li, N. Wollscheid, T. Buckup, A. Dreuw, N. Hampp and M. Motzkus, *J. Phys. Chem. A*, 2018, **122**, 7587–7597.
34 C. Calvino, *Chimia*, 2022, **76**, 816–825.
35 L. C. Chambers, C. Barner-Kowollik, L. Barner, L. Michalek and H. Frisch, *ACS Macro Lett.*, 2022, **11**, 532–536.
36 A. Garner and F. Wilkinson, *Chem. Phys. Lett.*, 1977, **45**, 432–435.
37 W.-M. Kwok, C. Ma and D. L. Phillips, *J. Am. Chem. Soc.*, 2008, **130**, 5131–5139.
38 T. Wolff and H. Görner, *J. Photochem. Photobiol., A*, 2010, **209**, 219–223.
39 D. K. Hohl, A.-C. Ferahian, L. Montero de Espinosa and C. Weder, *ACS Macro Lett.*, 2019, **8**, 1484–1490.
40 Y. Sun, Y. Ding, W. Zhou, X. Wang, C. Tan, Y. Matsumura, B. Ochiai and Q. Chu, *ACS Omega*, 2021, **6**, 28004–28011.
41 A. A. D'souza and R. Shegokar, *Expert Opin. Drug Delivery*, 2016, **13**, 1257–1275.
42 N. V. Tsarevsky, B. S. Sumerlin and K. Matyjaszewski, *Macromolecules*, 2005, **38**, 3558–3561.
43 C. Ozguc Onal and T. Nugay, *Des. Monomers Polym.*, 2017, **20**, 514–523.
44 C. Galli and L. Mandolini, *J. Chem. Soc., Chem. Commun.*, 1982, 251–253.
45 B. Dietrich, P. Viout and J.-M. Lehn, *Aspects de la chimie des composés macrocycliques*, EDP Sciences, Les Ulis, 1991.
46 P. Johnston, C. Braybrook and K. Saito, *Chem. Sci.*, 2012, **3**, 2301–2306.